Modelling diffraction during ray-tracing using the concept of energy flow lines

E. Hesse[1]
Science and Technology Research Institute, University of Hertfordshire, Hatfield, Herts, AL10 9AB, UK

Abstract

The ray tracing with diffraction on facets (RTDF) model is suitable for rapid computation of scattering on faceted dielectric objects such as ice crystals. It combines ray tracing with diffraction on flat facets. The model calculates diffraction using an approximation for the far field direction of the Poynting vector. In this paper an estimate based on an approximation by Prosser for the electric and magnetic fields describing diffraction at a slit is used to calculate energy flow lines and their far field deflection angle. Best-fit formulas describing the dependence of the far field deflection angle on the size parameter, angle of incidence, and the position of the flow line in the plane of the slit are derived and incorporated into the RTDF model. Phase functions for hexagonal columns are presented and compared with an analytic technique, the Separation of Variables Method, and Geometric Optics with projected area diffraction.

[1] Fax: +44 1707 284185.
E-mail: e.hesse@herts.ac.uk

1. Introduction

The importance of ice and mixed-phase clouds to the earth-atmosphere radiation balance and climate is well established. Though studied for many years, there is still a large uncertainty over the radiative properties of cirrus clouds. This is partly due to inadequate theoretical models of light scattering by the constituent ice crystals of realistic shapes and sizes.

Computations of light scattering properties for non-spheroidal particles based on exact methods like the Separation of Variables (SVM) Method, e.g.[1,2], *T*-matrix [3,4], Discrete Dipole Approximation (DDA) [5] and Discretized Mie Formalism (DMF) [6] have upper size parameter limits of applicability, depending on the method and the complexity of particle shape. This leaves a size parameter range which is covered neither by exact methods nor by Geometric Optics (GO). A modified Kirchhoff approximation (MKA) method has been introduced [7] to calculate far fields from classical Geometric Optics (GO) results, which encouraged the development of the Improved GO model [8]. The latter is, however, computationally expensive. For moderate values of the size parameter the Finite Difference Time Domain (FDTD) method can be used [9] but it too, puts severe demands on computational resources. Thus, despite its limitations, Geometric Optics (GO) combined with projected-area diffraction, e.g. [10], is still the most widely used model for moderate to large size parameters. Recently, diffraction on facets was introduced into a ray tracing model (RTDF) [11]-[13]. This method maintains the flexibility and computational inexpensiveness of GO while producing much improved results. Given the rapid and flexible computation offered by ray-tracing based models, it is possible to create 2D light scattering patterns for even very complex nonspherical crystals. Such patterns provide much more information than azimuthally averaged scattering data such as a phase function. In contrast to standard GO, the RTDF model can produce such patterns for fixed as well as averaged random orientation. 2D scattering patterns have been correctly predicted by the RTDF model [13], and it is therefore expected to become a suitable tool for particle characterization.

In this paper, an improvement of the ray deflection formula used in the RTDF model is presented. Resulting phase functions of hexagonal columns are compared with SVM [2], which is an analytical technique, and GO combined with projected area diffraction [10].

2. Computational methods

2.1. The Ray-Tracing with Diffraction on Facets model

Diffraction problems can be solved using Maxwell's equations, taking into account the polarization of the incident light as well as the electrical properties of the diffraction screen. Because of the mathematical difficulties involved, exact solutions have only been obtained for specific geometries and not too large dimensions of the scatterer compared to the wavelength. Maxwell's equations suggest an interpretation of diffraction and interference phenomena in terms of an undulation of the light path defined by the Poynting vector, which is complementary to the wavelet concept of Huygens [14-16]. This interpretation underlies the raytracing with diffraction on facets (RTDF) model [11-13]. During ray tracing each facet is treated as a slit (2D) or aperture (3D) at which each ray is bent according to the far field deflection angle, which an energy flow line through the slit would experience. In a 2D version, angular deflections of GO rays due to diffraction by a slit were calculated. In three dimensions, we assume that the deflection of a ray caused by diffraction by a facet can be modelled by two deflections each obeying the 2D rules. The formula for the calculation of the far field deflection angle used in [11-13] was based on calculations of energy flow lines passing a half plane [14,15] for perpendicular incidence. It was found that the far field

deflection angle of an energy flow line passing the half plane at a distance x could be approximated by

$$\varphi = \arctan\left(\frac{\lambda}{4\pi^2 x}\right) \quad (1)$$

[11]. Furthermore, the application of Eq. (1) leads to a far field energy density identical to the asymptotic form of the rigorous theory for the case of an unpolarized incident wave. In order to describe diffraction by a slit, this equation was modified to

$$\varphi = \arctan\left(\frac{\lambda}{4\pi^2}\left(\frac{1}{x} - \frac{1}{s-x}\right)\right) \quad (2)$$

where s is the width of the slit. This equation gives zero deflection for $x = s/2$ (middle position in the slit), and for positions close to the edges ($x \to 0$, $x \to s$) it reduces to the equation for a half-plane. A shortcoming of this formula is a singularity of the far field deflection angle at the centre of the slit, which results in an overestimation of the number of raypaths contributing at very low deflection angles. In this paper, energy flow lines passing a slit are calculated using an approximation obtained by Prosser [16], and formulae for the far field deflection are fitted to these results. The formulae are then implemented into the RTDF program and scattering by hexagonal columns is calculated as a test case.

The present implementation of the model is based upon the GO code by Macke *et al.* [10]. External diffraction, which is represented in the raytracing code [10] by Fraunhofer diffraction on the equal cross section circular aperture, was retained.

2.2. Diffraction by a slit approximated by superposition of solutions of Maxwell's equations for two half-planes

Prosser [16] stated that, if Φ_{+a}, and Φ_{-b} are the solutions of Maxwell's equations for half planes which extend from $x = a$ to $x = +\infty$ and from $x = b$ to $x = -\infty$, respectively, and Φ_f is the solution for free space, an approximate solution for the slit, Φ_{slit} , is given by

$$\Phi_{slit} = \Phi_{+a} + \Phi_{-b} - \Phi_f \quad (3)$$

He showed that this equation approximately satisfies the electromagnetic boundary conditions for a slit in an infinite, perfectly conducting plane. Small deviations from the boundary condition $E_x = 0$ in the conducting plane occur close to the slit edges. The approximate solution should generally be satisfactory in cases where the slit widths are greater than one wavelength [16].

We consider a slit with edges in Cartesian coordinates at $x = 0$ and $x = -s$ in an infinite plane at $y = 0$. This corresponds to indices $a = +0$ and $b = -s$ in Eq. (3),

$$\Phi_{slit} = \Phi_{+0} + \Phi_{-(-s)} - \Phi_f \quad (3a)$$

Born and Wolf [14] state Sommerfeld's equations for the E- and H-fields for diffraction at a half-plane placed in Cartesian coordinates at $y = 0$, $x \geq 0$. (In the following, index 1 is used for this half plane.) In the case of E-polarization the incident electric field vector is assumed to be parallel to the edges of the slit and its components can be specified as $E_{x1}^{(i)} = E_{y1}^{(i)} = 0$ and

$$E_{z1}^{(i)} = Ae^{-ikr_1\cos(\theta_1 - \alpha_0)} \quad (4)$$

where r_1 and θ_1 are polar coordinates related to x and y by the equations $x = r_1 \cdot \cos(\theta_1)$, $y = r_1 \cdot \sin(\theta_1)$, α_0 is the angle between the positive x-axis and the direction of propagation (Fig.1), k and ε_0 are the wave number and vacuum permittivity, respectively. Eq. (4) is normalized to $A = 1$. (The Gaussian system of units as applied in [14] is used).

The complete field E_{z1} can be written in the form

$$E_{z1} = \frac{e^{-\frac{1}{4}i\pi}}{\sqrt{\pi}}\left\{e^{-ikr_1\cos(\theta_1-\alpha_0)}F[-\sqrt{2kr_1}\cos\frac{1}{2}(\theta_1-\alpha_0)] - e^{-ikr_1\cos(\theta_1+\alpha_0)}F[-\sqrt{2kr_1}\cos\frac{1}{2}(\theta_1+\alpha_0)]\right\} \quad (5)$$

where $F[a] = \int_a^\infty e^{i\xi^2} d\xi$ is the complex Fresnel integral. The polar angle θ_1 has values $0 \le \theta < 2\pi$.

The following equations relate the polar and Cartesian coordinates:

$$\theta_1 = \arctan\left(\frac{y}{x}\right) \quad for\ y > 0$$

$$\theta_1 = \arctan\left(\frac{y}{x}\right) + 2\pi \quad for\ y < 0 \quad (6)$$

$$r_1 = \sqrt{x^2 + y^2}$$

The complete field E_{z2} for a half-plane at $x \le -s$ is given by:

$$E_{z2} = \frac{e^{-\frac{1}{4}i\pi}}{\sqrt{\pi}}\left\{e^{-ikr_2\cos(\theta_2+\alpha_0-\pi)}F\left[-\sqrt{2kr_2}\cos\frac{1}{2}(\theta_2+\alpha_0-\pi)\right] - e^{-ikr_2\cos(\theta_2+\alpha_0-\pi)}F\left[-\sqrt{2kr_2}\cos\frac{1}{2}(\theta_2-\alpha_0+\pi)\right]\right\} \quad (7)$$

with

$$\theta_2 = \arctan\left(\frac{y}{-(x+s)}\right) \quad for\ y > 0$$

$$\theta_2 = \arctan\left(\frac{y}{-(x+s)}\right) + 2\pi \quad for\ y < 0 \quad (8)$$

$$r_2 = \sqrt{(x+s)^2 + y^2}$$

The electric field term corresponding to the solution for free space Φ_f in Eq.(3) is given by Eq. (4). With a time factor $\exp(-i\omega t)$ suppressed the 2nd Maxwell's equation is

$$\nabla \times \vec{\mathrm{E}} = ik\vec{\mathrm{H}} \quad (9)$$

where μ_0 is the vacuum permeability. Equating to zero all partial derivatives with respect to z, this may be split up into

$$H_x = \frac{1}{ik}\frac{\partial E_z}{\partial y}, \quad H_y = -\frac{1}{ik}\frac{\partial E_z}{\partial x} \quad (10)$$

The time-averaged Poynting vector is given by

$$\langle \vec{\mathrm{S}} \rangle = \frac{1}{2}\Re\left(\vec{\mathrm{E}} \times \vec{\mathrm{H}}^*\right) = \frac{1}{2}\Re(-E_z H_y{}^*, E_z H_x{}^*, 0) \quad (11)$$

The energy flow lines can be obtained by solving the differential equation:

$$\frac{\mathrm{d}x}{\mathrm{d}y} = \frac{\langle S(x(y), y)\rangle_x}{\langle S(x(y), y)\rangle_y} \quad (12)$$

2.2.1. Perpendicular incidence

Energy flow lines for light incident perpendicularly to a conducting plane containing a long slit, i.e. $\alpha_0 = \pi/2$, calculated using Eq. (11) for starting points at $y = 0$, are shown in Figs. 2(a) and (b). The calculations are for *E*-polarized incident light, i.e. the incident electric field vector is assumed to be parallel to the long edges of the slit. The size parameter $\chi = ks/2$ has a value of 50. The dash-dotted line at $x/\lambda = -100/2\pi = -7.958$ corresponds to the slit centre. In the

close-up (Fig. 2(b)) the strong undulations of the energy flow lines near the slit plane are clearly visible. In the far field, the energy flow lines are straight and include an angle with the direction of propagation of the incident light, which is called the far field deflection angle φ. It increases with decreasing distance of the starting point from the slit edge. Looking at the distribution in the far field of energy flow lines with equally spaced starting points at $-x_0/\lambda = -x/\lambda$ ($y = 0$) = 0.1, 0.2,…,1.0, we find two groups of densely spaced flow lines, $-x_0/\lambda$ = 0.5, 0.6 and 0.7, and $-x_0/\lambda$ = 0.8, 0.9 and 1.0, and a gap between them. The far field deflection angles of the energy flow lines with $-x_0/\lambda$ = 0.7 and 0.8 are 4.72° and 3.09°, respectively. The gap between them is due to the flattening out of the last undulation of the energy flow lines with decreasing $|x_0/\lambda|$ and corresponds to the first minimum of the Fraunhofer diffraction pattern at 3.60°. The second minimum of the Fraunhofer diffraction pattern at 7.22° is positioned in the large gap between the energy flow lines with $-x_0/\lambda$ = 0.5 and 0.4, respectively, and so on. This is in agreement with Prosser's statement [11] that the redistribution of energy due to the nonlinear trajectory is what is observed as a diffraction or interference pattern. Energy flow lines were calculated for size parameters 10, 25, 100 and 200 as well.

Fig. 3 shows a logarithmic plot of the far field deflection angle vs. $X = -2x_0/s$. The factor $2/s$ was used in order to allow easy comparison of graphs for different slit widths. It can be seen that for all size parameters the far field deflection angle decreases monotonically towards the middle of the slit. For $X \to 0$ or 1 it approaches $\pi/2$ or 0, respectively. Close to $X = 0$ the graphs show a steep decrease, followed by a narrow shoulder in the region X = 0.07...0.15 and a slow decay towards the middle of the slit. In general, the angular density of energy flow lines in the far field is proportional to the angular intensity of the scattered light and inversely proportional to the modulus of the slope of the $\varphi(-2x_0/s)$ curve, i.e. to $|d\varphi/dx|$. The steep slope to the right of the shoulder corresponds to the first minimum of the Fraunhofer diffraction pattern. The angular position of the first minimum in the corresponding Fraunhofer pattern is indicated by thin horizontal lines on the right hand side of the ordinate in Fig. 3. For χ =100 and 200 the second diffraction minimum is discernible, too.

Next, we wish to find a suitable fit for $\varphi(x_0, s, \lambda)$ in order to replace Eq. (2) in the RTDF model. The dotted line in Fig. 3 corresponds to Eq. (2) for $s = \chi = 200$. This equation was conjectured from calculated values of $\varphi(x_0/\lambda)$ for a half-plane. Eq. (2) and the calculated $\varphi(x_0, s, \lambda)$ have the same limits for $x_0 \to 0$ and $x_0 \to s/2$. However, Eq. (2) gives a steeper decay of the far field deflection angle with distance from the slit edge. The best fit for X larger then the values corresponding to the angular range around the first diffraction minimum to the equation

$$\varphi_r = \arctan\left(\frac{P_2 \cdot \lambda}{2\pi^2 s}\left(\frac{1}{X^{P_1}} - \frac{1}{(2-X)^{P_1}}\right)\right) \tag{13}$$

gives P_1 = 1.5e-4 and P_2=32184. The fits are shown in Fig. 3 as dashed lines. There is now good agreement with the calculated values $\varphi(x_0, s, \lambda)$ for the largest fraction of the rays, i.e. those forming the central maximum of the diffraction pattern. Furthermore, it was found that the function

$$\varphi_l = \arctan\left(\frac{\lambda}{\pi^2 s X}\right) = \arctan\left(\frac{\lambda}{2\pi^2 x_0}\right) \tag{14}$$

is a good fit to the envelope of the Fraunhofer diffraction pattern away from the first interference maximum. Eqs. (13) and / or (14) need to be modified in such a way, that the resulting function φ, consisting of φ_l for $X<X_s$ and φ_r for $X>X_s$, is continuous and

approximates the calculated values around X_s, which is the X-coordinate of the intersection point of φ_l and φ_r. To achieve this, additional terms were introduced into Eq. (13):

$$\varphi_r^* = \arctan\left(\frac{\lambda}{2\pi^2 s}\left(P_2\left(\frac{1}{X^{P_1}} - \frac{1}{(2-X)^{P_1}}\right) + P_4\left(\frac{1}{X^{P_3}} - \frac{1}{(2-X)^{P_3}}\right)\right)\right) \tag{15}$$

The following fit results were obtained: P_1 = 9.9e-6; P_2 = 4.854e5; P_3 =7.45; P_4 = 1.113e-7. The intersection points of φ_r^* and φ_l are at X_s = 0.0883, i.e. X_s is size parameter independent within the investigated range of parameters. In Fig. 3 the resulting fit functions φ_r^* and φ_l are plotted as continuous and dash dotted lines, respectively. Fig. 4 shows the far field angular intensity distributions for diffraction at slits of size parameters 25 and 100 calculated using Eqs. (14) and (15) with the parameters given above. There is good agreement for the central peak of the Fraunhofer distribution as well as for the angular distribution averaged over local maxima and minima. The sharp edges around the first diffraction minimum are related to the corresponding step of the $\varphi(X)$ curve. Overall, the modelling result is much improved compared to Eq. (2).

2.2.2. Oblique incidence

Calculated far field deflection angles of energy flow lines for oblique incidence onto a slit for different combinations $[x_0,s]$ and $\lambda = \pi$ were calculated. Figs. 5(a) and (b) show logarithmic plots $\varphi(X)$ for $s = \chi = 100$ for a range of incident angles $\alpha_0 < \pi/2$ and $\alpha_0 > \pi/2$, respectively. For energy flow line calculations equal phase at both slit edges is required (Eqs. (5) and (7)). Therefore, the conditions

$$\begin{aligned} &\cos\alpha_0 = \frac{n\lambda}{s} \quad \forall\, \alpha_0 < \frac{\pi}{2} \\ &\cos(\pi - \alpha_0) = \frac{n\lambda}{s} \quad \forall\, \alpha_0 > \frac{\pi}{2} \end{aligned} \tag{16}$$

need to be fulfilled, which means that for each ratio λ/s calculations can only be carried out for a certain set of angles α_0. As done in the discussion of Fig. 3, we consider different regions X which can be described by particular fit functions. The region of X larger then the values corresponding to the angular range around the first diffraction minimum can be described by a modified version of Eq. (13), keeping the values of P_1 and P_2.

$$\varphi_r = \arctan\left(\frac{P_2 \cdot \lambda}{2\pi^2 s \sin\alpha_0}\left(\frac{1}{X^{P_1}} - \frac{1}{(2-X)^{P_1}}\right)\right) \tag{17}$$

In the following we introduce an equation analogous to Eq. (15), which covers the X region described by φ_r in Eq. (17) as well as the first diffraction minimum.

$$\varphi_r^* = \varphi_r + \varphi_{\min} \tag{18}$$

$$\varphi_{\min} = \frac{\pi - \alpha_0}{\pi/2} \arctan\left(\frac{P_2^* \cdot \lambda}{2\pi^2 s \sin\alpha_0}\left(\frac{1}{X^{P_1^*}} - \frac{1}{(2-X)^{P_1^*}}\right)\right) \tag{19}$$

For $\alpha_0 < \pi/2$ the position X corresponding to the first Fraunhofer diffraction minimum depends strongly on the incident angle. This is covered by P_1^*.

$$\begin{aligned} &P_1^* = A(\pi/2 - \alpha_0)^B \tan(\pi/2 + \alpha_0) + 20.285 \\ &A = -18.30967(s/\lambda)^{-0.19685(s/\lambda)^{0.3904}} \\ &B = 0.01237(s/\lambda)^{2.5964(s/\lambda)^{-0.13048}} \\ &P_2^* = 1e-20 \end{aligned} \tag{20a}$$

For $\alpha_0 > \pi/2$, the variation of the X-position of the first Fraunhofer diffraction minimum is negligible. Therefore P_1^* and P_2^* are set to be constant.

$$P_1^* = 20.285$$
$$P_2^* = 1e-20 \tag{20b}$$

Eqs. (21a) and (21b) are suitable fits $\varphi(X)$ for positions X close to the edges for $\alpha_0 < \pi/2$ or $\alpha_0 > \pi/2$, respectively.

$$\varphi_l = \frac{\pi - \alpha_0}{\pi/2} \arctan\left(\frac{Q}{\pi^2 X^{\cos^2\alpha_0 + 1}}\right)$$
$$Q = \frac{-0.62797(s/\lambda)^{0.18009} \sin^2(\alpha_0 + 0.628)\cos\alpha_0 + 1}{(s/\lambda)\sin\alpha_0} \tag{21a}$$

$$\varphi_l = \frac{\pi - \alpha_0}{\pi/2} \arctan\left(\frac{Q}{\pi^2 X}\right)$$
$$Q = \frac{(1.36238 - 0.00607 s/\lambda)(\tan(\alpha_0 + \pi/2))^{0.98518(s/\lambda)^{0.07908}} + 1}{(s/\lambda)\sin\alpha_0} \tag{21b}$$

Note that for $\alpha_0 = \pi/2$ Eq. (21) is identical to Eq. (14), and Eq. (20) gives results very similar to Eq. (15), as can be seen in Figs. 4.

2.3. Implementation of the improved diffraction formula in the RTDF model

Eqs. (17-21) were implemented in the RTDF model. The results are compared to computations using a generalization of SVM [2], which is an analytical technique, and GO combined with projected area diffraction [10]. Fig. 6 shows randomized phase functions for hexagonal columns, with refractive index n = 1.31 for size parameters $\chi = 2\pi a/\lambda$ equal to 12, 30 and 50. The aspect ratio of the column $L/2a$ is 10, where L is the column length and $2a$ its diameter. Due to the approximation involved in the SVM calculation, the orientations are restricted, so that the column axis is at least a certain angle away from the direction of the incident light. For the investigated size parameters, this angle is in the range of 6.2° to 13.0°. RTDF and GO calculations were carried out for the same angular restrictions. The RTDF results approximate those by SVM much better than GO over the whole angular range, and in particular in near direct forward and backscattering, in the halo region and in the backscattering region between 142° and 160°. Note that there is no halo for χ =12.

3. Summary

The RTDF model is suitable for rapid computation of scattering on faceted dielectric objects such as ice crystals. It combines ray tracing with diffraction on flat facets. The model calculates diffraction using an approximation for the far field direction of the Poynting vector. The angle of diffraction of an externally reflected or outward refracted ray is calculated from the ray's proximity to the facet edges. In this paper, an estimate for the electric and magnetic fields describing diffraction at a slit based on an approximation by Prosser [16] was used to calculate energy flow lines and their far field deflection angle. The calculations show a distinct depletion of the angular density of energy flow lines in the far field around the angular position of the first minimum of the Fraunhofer diffraction pattern as well as weaker reductions at higher order diffraction minima. This is in agreement with Prosser's statement [16], that the redistribution of energy due to the nonlinear trajectory is what is observed as a diffraction or interference pattern. Best-fit equations describing the dependence of the far field

deflection angle on the size parameter and the position of the flow line in the plane of the slit have been obtained. This method avoids the singularity at the centre of the slit that occurred in an earlier approach based on results of rigorous diffraction theory for diffraction of a plane wave by a half-plane. The new approach models the shape of the zero-order diffraction maximum accurately and fits the envelope of the Fraunhofer diffraction pattern. The new ray bending equations have been implemented in the RTDF program, increasing the computational overhead only slightly. Phase functions for near random orientation of hexagonal columns are presented and compared with SVM [2], which is an analytical method, and with GO with projected area diffraction [10]. The RTDF results approximate those by SVM much better than GO over the whole angular range, and in particular in near direct forward and backscattering, in the halo region and in the backscattering region between 142° and 160°. The method can be applied to arbitrary faceted objects and can be used to calculate 2D scattering patterns for fixed and random orientation.

Acknowledgement

This research was supported by the Natural Environment Research Council of the UK. The author is grateful to A. Macke for providing the ray tracing code, to S. Havemann for the SVM data and to Z.J. Ulanowski and A.J. Baran for valuable discussions.

References

[1] Rother, T, Schmidt, K, Havemann, S. Light scattering on hexagonal ice columns. J Opt Soc Am A 2001;18:2512-2517.

[2] Havemann S, Rother T, Schmidt K. Light scattering by hexagonal ice crystals. In: Mishchenko MI, Travis LD, Hovenier JW, editors. Conference on Light Scattering by Nonspherical Particles: Theory, Measurements and Applications, 29th September-1st October 1998. New York: American Meteorological Society, p.253-6.

[3] Mishchenko, MI, Videen, G., Babenko, VA, Khlebtsov, NG, Wriedt, T. T-matrix theory of electromagnetic scattering by particles and its applications: a comprehensive reference database. J Quantit Spectrosc Radiat Transf 2004;88:357-406.

[4] Mishchenko, MI, Videen, G., Babenko, VA, Khlebtsov, NG, Wriedt, T. Comprehensive T-matrix reference database: A 2004-06 update. J Quantit Spectrosc Radiat Transf 2007;106:304-324.

[5] Yurkin, MA, Hoekstra, AG. The discrete dipole approximation: An overview and recent developments. J Quantit Spectrosc Radiat Transf 2007;106:558-589.

[6] Rother, T, Schmidt, K. The discretized Mie-formalism for electromagnetic scattering – Summary. Journal of electromagnetic waves and applications 1997;11:1619-1625.

[7] Muinonen K. Scattering of light by crystals: a modified Kirchhoff approximation. Appl Opt 1989; 28: 3044-3050.

[8] Yang P, Liou KN. Geometric-optics-integral equation method for light scattering by nonspherical ice crystals. Appl Opt 1996; 35, 6568-6584.

[9] Yang P, Liou KN. In: Mishchenko MI, Hovenier JW, Travis LD, editors. Light scattering by nonspherical particles, New York: Academic Press, 1999. p. 173-221.

[10] Macke A, Mueller J, Raschke E. Single scattering properties of atmospheric ice crystals. J Atmos Sci 1996; 53: 2813-2825.

[11] Hesse E, Ulanowski Z. Scattering from long prisms using ray tracing combined with diffraction on facets. 6th Conference on Light Scattering by Nonspherical Particles,

Theory, Measurements, and Applications, March 4-8, 2002, Gainesville, Florida, USA, J Quantit Spectrosc Radiat Transf 2003; 79-80C: 721-732
[12] Hesse E, Ulanowski Z, Havemann S. Scattering from long prisms: A comparison between ray tracing combined with diffraction on facets and SVM. Proceedings 7th Conference on Electomagnetic and Light Scattering by Nonspherical Particles, Theory, Measurements, and Applications, Sept. 8-12, 2003, Bremen, Germany, p. 119-122.
[13] Clarke AJM, Hesse E, Ulanowski Zand Kaye PH. A 3D implementation of ray-tracing with diffraction on facets: Verification and a potential application. J Quantit Spectrosc Radiat Transf 2006; 100: 103-114.
[14] Born M, Wolf E. Principles of optics, 7th ed. Cambridge: CUP, 1999.
[15] Braunbek W, Laukien G. Einzelheiten zur Halbebenen-Beugung. Optik, 1952; 9: 174-179.
[16] Prosser RD. The interpretation of diffraction and interference in terms of energy flow. Int J Theoret Phys 1976; 15: 169-180.

Captions of figures

Fig. 1: *E*-polarized plane wave incident on perfectly conducting half-plane.

Fig. 2: (a) Time-averaged energy flow lines for perpendicular incidence of *E*-polarized light on a slit of size parameter 50 at $y = 0$. The numbers inside the frame indicate the distance $-x_0/\lambda$ in the slit plane between the flow lines and the right slit edge (The slit centre corresponds to $-x_0/\lambda = 50/\pi$). The arrow indicates the first minimum of the Fraunhofer diffraction pattern. (b) close-up.

Fig. 3: Logarithmic plot of the far field deflection angle of the energy flow lines vs. $X=-2x_0/s$, where $-x_0$ is the distance from the edge at $y = 0$ at which the energy flow lines pass, and fit functions Eq.(2), Eqs.(13-15).

Fig. 4: Far field angular intensity distributions for diffraction at a slit for size parameters 25 (a) and 100 (b) calculated using Eqs. (14-15) and (17-21) respectively, and comparison with Eq. (2) and the Fraunhofer diffraction pattern.

Fig. 5: (a) Logarithmic plots $\varphi(X)$ for $s = \chi = 100$ for a range of incident angles $\alpha_0 < \pi/2$ (a) and $\alpha_0 > \pi/2$ (b), and fits Eqs. (17-20) and Eq. (21).

Fig. 6: Phase functions for hexagonal columns with refractive index $n = 1.31$, aspect ratio $L/2a = 10$, and size parameters $\chi = 2a/\lambda$ of (a) $\chi = 12$, (b) $\chi = 30$ and (c) $\chi = 50$, respectively, for near random orientation calculated using RTDF with ray deflection formulas Eqs. (17) to (21) in comparison with SVM [12] and GO with projected area diffraction [10] results.

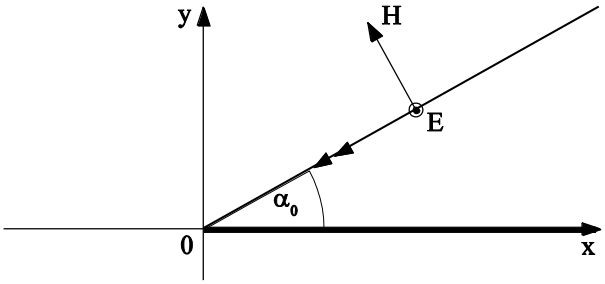

Fig. 1

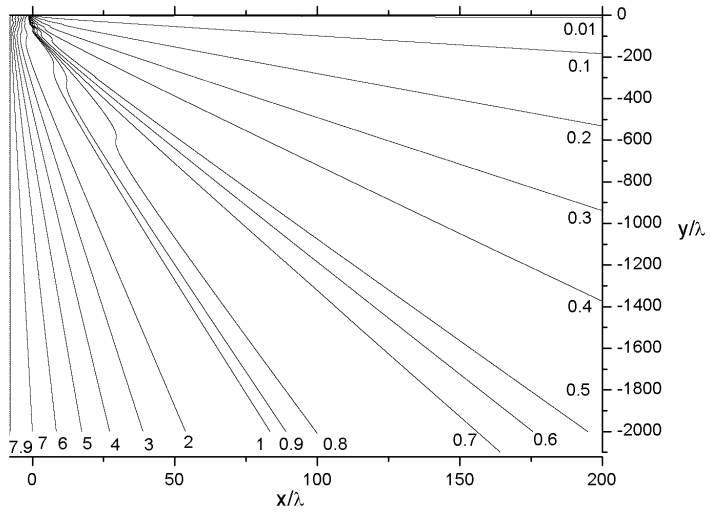

Fig. 2a

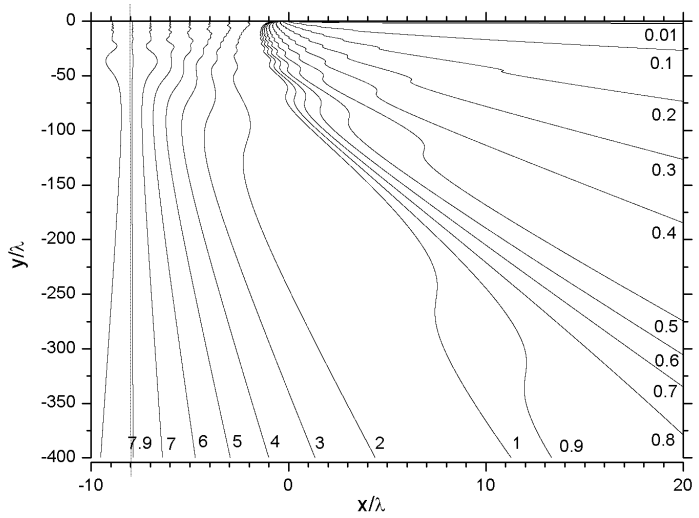

Fig. 2b

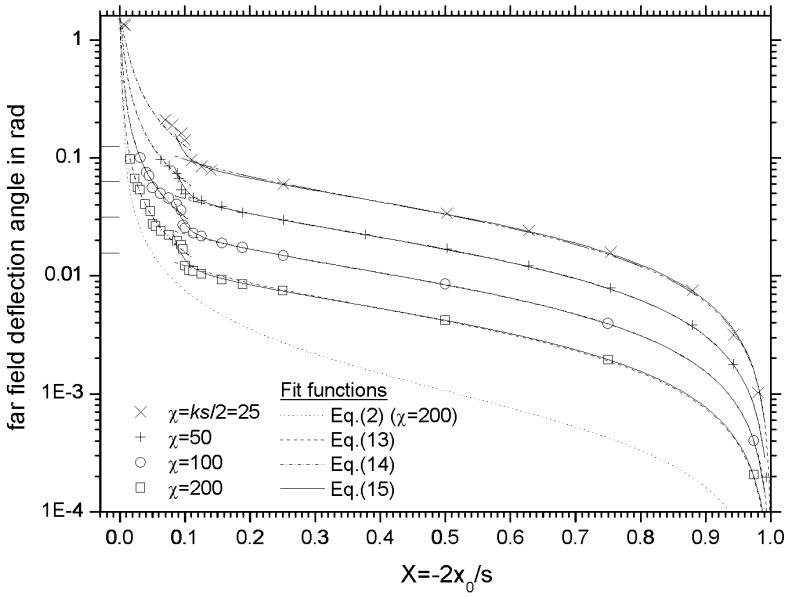

Fig.3

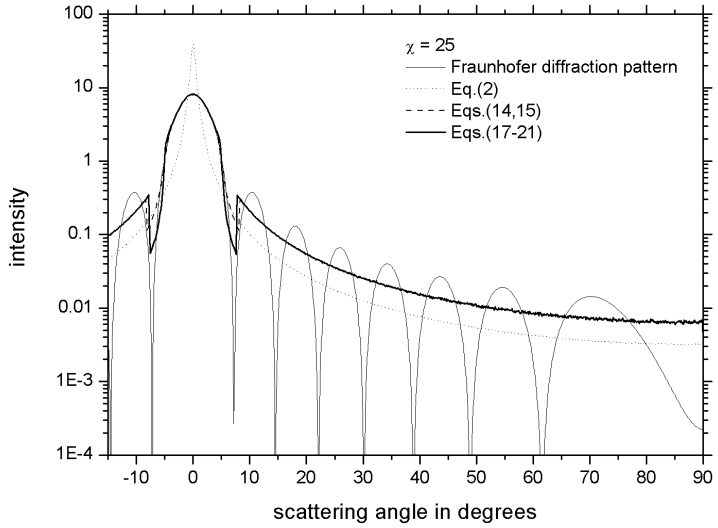

Fig.4a

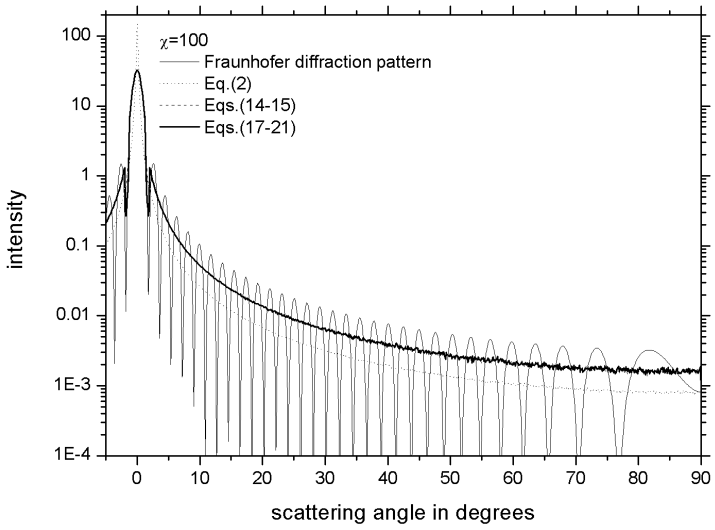

Fig.4b

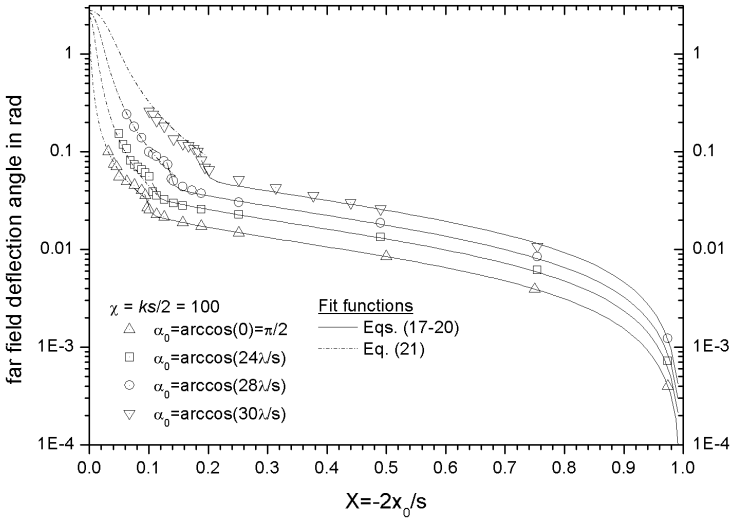
far field deflection angle in rad
1
0.1
0.01
1E-3
1E-4
0.0
0.1
0.2
0.3
0.4
0.5
0.6
0.7
0.8
0.9
1.0
X=-2x0/s
χ = ks/2 = 100
α0=arccos(0)=π/2
α0=arccos(24λ/s)
α0=arccos(28λ/s)
α0=arccos(30λ/s)
Fit functions
Eqs. (17-20)
Eq. (21)

Fig5a

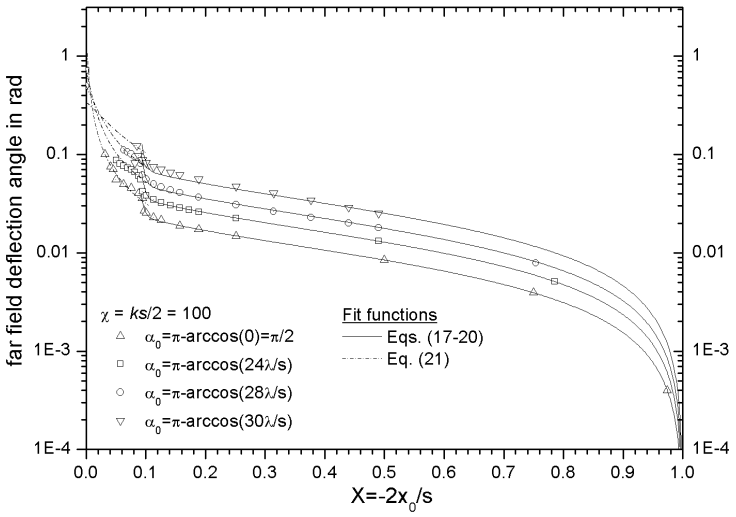
far field deflection angle in rad
1
0.1
0.01
1E-3
1E-4
0.0
0.1
0.2
0.3
0.4
0.5
0.6
0.7
0.8
0.9
1.0
X=-2x0/s
χ = ks/2 = 100
α0=π-arccos(0)=π/2
α0=π-arccos(24λ/s)
α0=π-arccos(28λ/s)
α0=π-arccos(30λ/s)
Fit functions
Eqs. (17-20)
Eq. (21)

Fig.5b

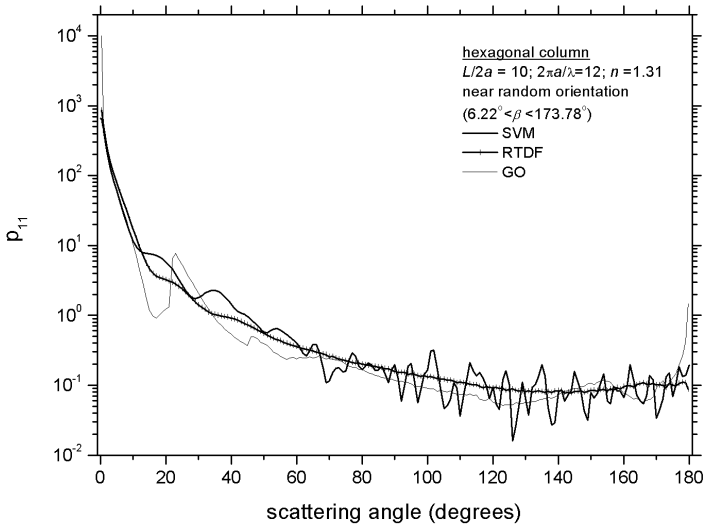

Fig6a

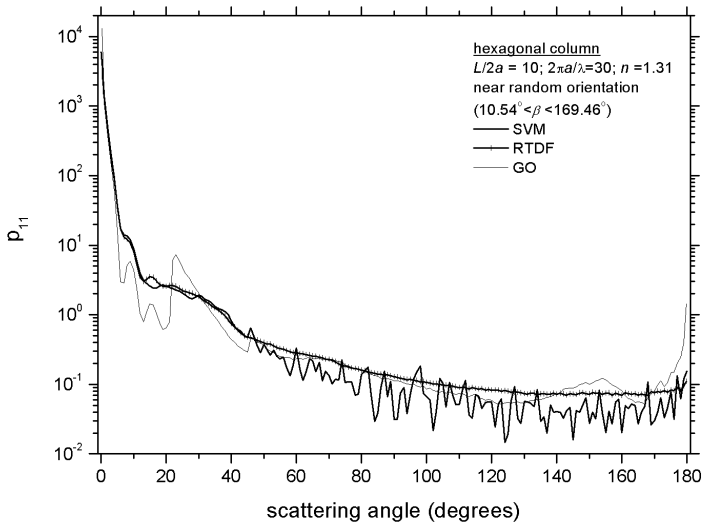

Fig. 6b

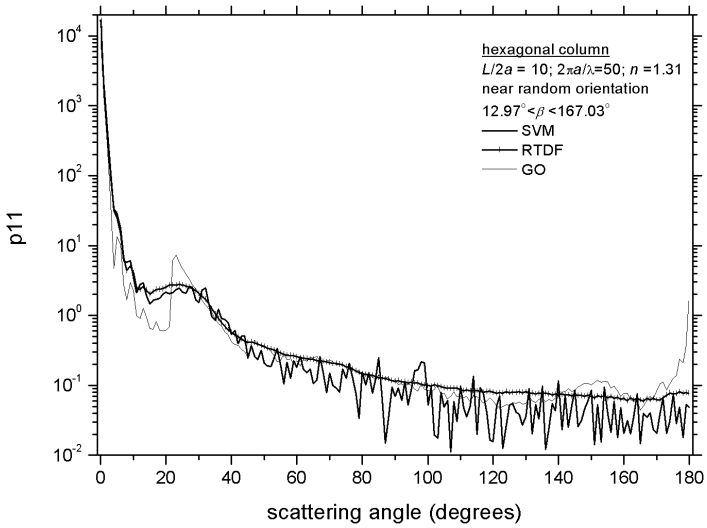

Fig. 6c